Article

Functional Integration of Catalysts with Si Nanowire Photocathodes for Efficient Utilization of Photogenerated Charge Carriers

Sung Yul Lim,* Daye Seo, Min Seok Jang, and Taek Dong Chung*

Cite This: *ACS Omega* 2021, 6, 22311−22316

Read Online

ACCESS | Metrics & More | Article Recommendations | SI Supporting Information

ABSTRACT: Low-cost catalysts with high activity and durability are necessary to achieve efficient large-scale energy conversion in photoelectrochemical cell (PEC) systems. An additional factor that governs the construction of photoelectrodes for PECs is the spatial control of the catalysts for efficient utilization of photogenerated charge carriers. Here, we demonstrate spatial decoupling of the light-absorbing and catalytic components in hierarchically structured Si-based photocathodes for the hydrogen evolution reaction (HER). By simply modifying a well-known metal-assisted chemical etching procedure, we fabricated a Si nanowire (NW) array-based photocathode with Ag−Pt catalysts at the base and small amounts of the Pt catalyst at the NW tips. This approach simultaneously mitigates the parasitic light absorption by the catalytic layers and recombination of charge carriers owing to the long transport distance, resulting in improved photoelectrochemical HER performance under simulated AM 1.5G illumination.
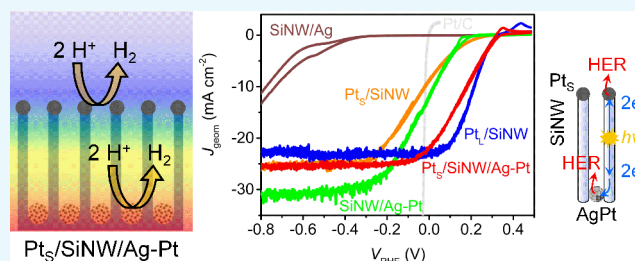
1. INTRODUCTION

The development of electrochemically active, durable, and cost-effective catalysts for the conversion of water (H_2O) into hydrogen (H_2) is beneficial for realizing a carbon-neutral, sustainable society. To achieve this goal, solar-driven water splitting devices have been widely used because they alleviate the electrical energy input required to produce H_2.[1−10] Although highly active catalysts are indispensable for an efficient hydrogen evolution reaction (HER) on the semiconductor surface (light absorber), parasitic light absorption by optically opaque catalysts on the surface of light absorbers reduces the amount of incident photons that reaches them.[11,12] Since light must reach the absorber through the catalytic layers to generate charge carriers from excitons, it is important to integrate the catalysts onto the surface of photoelectrodes with controlled spatial distribution for efficient photon management. Otherwise, there will be an unavoidable negative correlation between catalyst loading and photoelectrochemical performance.[13]

Hierarchically structured Si-based light absorbers are popular, high-performing photocathodes for the HER owing to their high photon-absorption capability, abundance of Si, and well-developed processing technologies.[14,15] Silicon nanowires (SiNWs) can be easily and scalably fabricated by simple wet-chemical procedures, and high-aspect-ratio NW arrays can be readily fabricated by metal-assisted chemical etching (MACE).[16−18] Although SiNWs themselves exhibit high photon absorption over a wide wavelength range, SiNW-based photocathodes often suffer from deteriorated saturated photocurrent density (J_{SC}) after the deposition of a catalyst.[17] The chemical deposition of metal precursors to form

conformal catalytic layers on high-aspect-ratio structures is often limited by diffusion in solution, which results in nonuniform nucleation of catalyst particles on the tips of the SiNWs.[14,17] Therefore, unless the deposition conditions are carefully controlled, the catalytic particles on top of the SiNWs would lead to diminished photon absorption by the SiNWs as the light absorber underneath them. In addition, the thick catalysts deposited on the tips of NWs with a high-curvature surface often undergo severe mechanical delamination during the HER due to vigorous gas bubble formation.[17,19]

To simultaneously achieve high photon absorption and catalytic activity of SiNW photoelectrodes, one promising method involves spatial and functional decoupling of the regions responsible for optical absorption and catalytic conversion by selective control of the location of the catalysts on the vertically aligned NW surface, leaving the bare semiconductor surface as a window for photon absorption while maintaining the adequate catalyst amounts.[13,14,20] This can be achieved using templated (electro)chemical techniques, such as on-wire lithography,[21] coaxial lithography,[22] and three-dimensional electrochemical axial lithography.[23] Although these techniques guarantee the precise control of the spatial
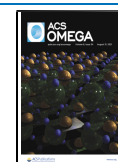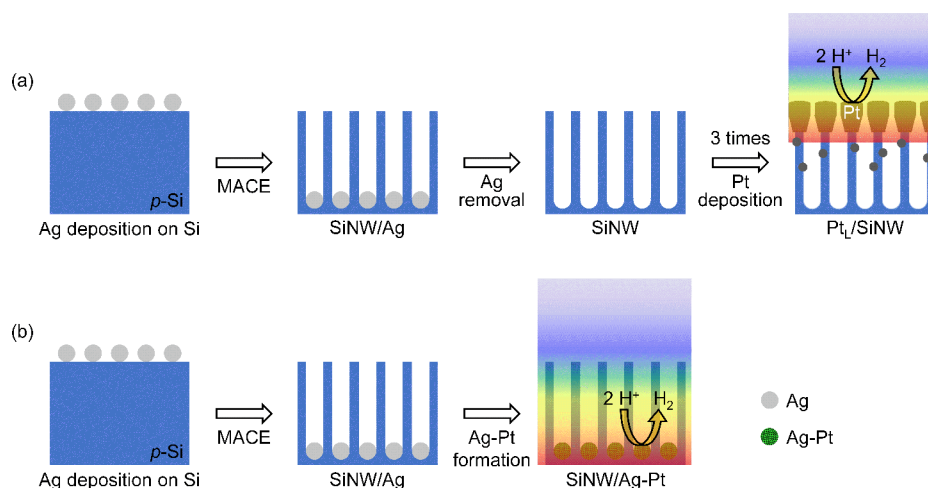
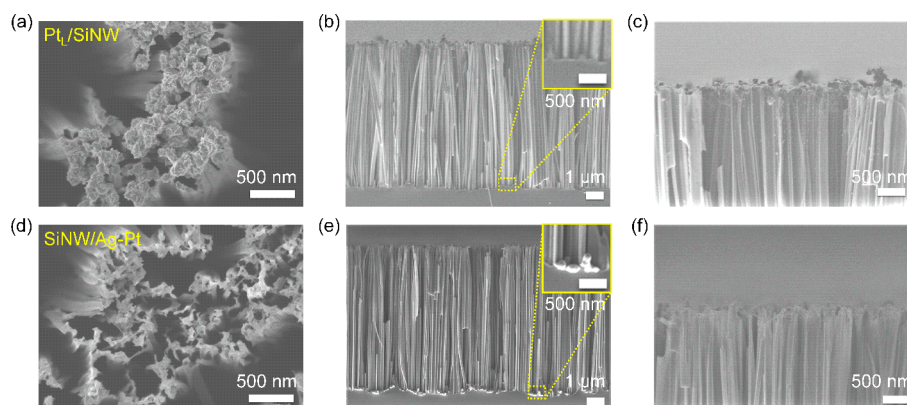**Figure 1.** Schematic illustration of the preparation of (a) Pt_L/SiNW and (b) SiNW/Ag−Pt photocathodes for the HER.

Figure 2. SEM images of (a−c) Pt_L/SiNW and (d−f) SiNW/Ag−Pt. (a and d) Plane view and (b, c, e, and f) cross-sectional view of the SiNW-based photocathodes. The insets in (b) and (e) show that the SiNW/Ag−Pt photocathodes contain catalyst particles at the base of the SiNWs, while Pt_L/SiNW possesses catalysts only at the tips of the NWs (c). The durations of the NW etching and galvanic exchange to form Ag−Pt were 30 and 2 min, respectively.

location of catalysts on the NWs, they require complicated fabrication procedures using high-vacuum equipment.

Herein, we demonstrate a simple chemical approach for the spatial control of catalysts on SiNW photocathodes to decouple the light absorption and catalytic activity. Ag−Pt catalysts were integrated at the base of a high-aspect-ratio SiNW array by slightly modifying the conventional MACE protocol for the fabrication of SiNW photocathodes. Such Ag−Pt catalysts are beneficial for reducing expensive elements while maintaining high catalytic activity toward the HER.[24] According to our previous studies, Pt is more prone to parasitic visible light absorption than Ag.[25] Although low amounts of Pt are enough in terms of electrocatalytic activity for the HER, fine control of the spatial distribution of Pt is critical. After optimization of the NW length and Ag−Pt composition in the catalyst at the NW base, a small amount of pure Pt was additionally deposited on the NW tips to reduce the distance for transport of the photogenerated electrons to the catalytic sites. Thus, we achieved a marginally higher J_{SC} under the same open-circuit potential (V_{OC}) at only one-third of the Pt loading compared with that of a conventional SiNW photocathode decorated only with pure Pt particles on the tips of the NWs.[17] In addition, smaller amounts of Pt deposited at the tips improved the long-term stability by enhancing the physical adhesion between the metallic particles and Si. This may

originate from the lower internal strain associated with smaller catalytic particles, allowing them to endure the evolution of H_2 gas bubbles.[26] Our work will provide valuable insights for the design of better photoelectrochemical cell (PEC)-based chemical fuel production systems.

2. RESULTS AND DISCUSSION

Figure 1 schematically presents the fabrication process of the SiNW-array photocathodes with spatially controlled catalyst particles. Figure 1a shows the conventional method for preparing SiNW photocathodes (Pt_L/SiNW) based on MACE. Ag catalyzes the downward Si surface etching according to the reaction Si + $2H_2O_2$ + $6F^-$ + $4H^+$ → SiF_6^{2-} + $4H_2O$ and is eventually located at the base after the NW arrays form.[27] In most of the previously reported syntheses of SiNW arrays by MACE as photocathodes for the HER, the Ag particles at the base were removed before the deposition of catalysts.[17] For a benchmark photocathode, we deposited Pt catalysts dominantly at the SiNW tips by immersing the electrodes into aqueous HF solutions containing Pt^{2+} ions (see the details in the Supporting Information) by following the removal of Ag at the base. Pt deposition was conducted three times, herein denoted Pt_L/SiNW. In this method, the dominant Pt deposition at the SiNW tips is due to the depletion of metal precursor ions near
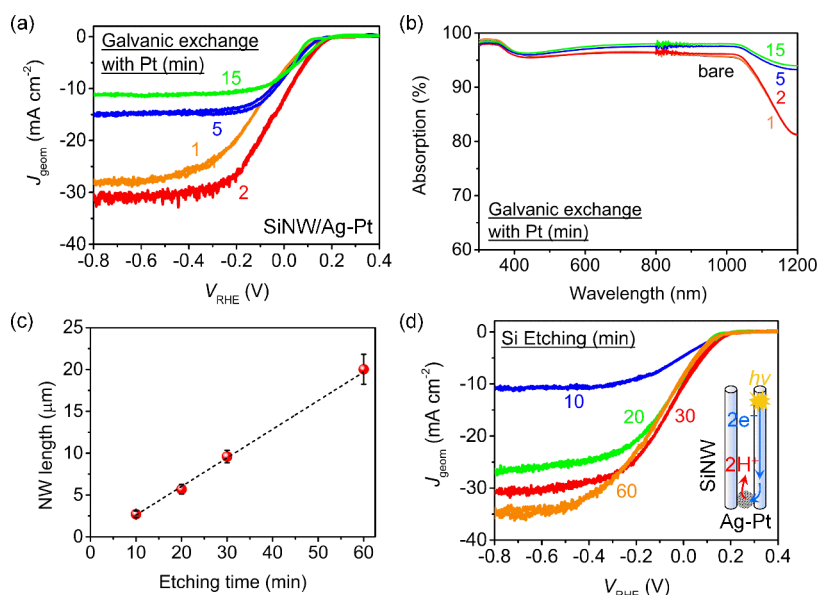
Figure 3. (a) CVs and (b) absorption spectra for the SiNW/Ag−Pt photocathodes prepared with different galvanic exchange reaction times. The black line indicates the spectrum of bare SiNW. (c) Correlation between the NW length and the etching time. (d) CVs for the evaluation of the photoelectrochemical HER performance of the SiNW/Ag−Pt photocathodes with different NW lengths by varying the etching time. The voltammograms were acquired under simulated AM 1.5G illumination (100 mW cm^{-2}) with H$_2$-purged 0.5 M H$_2$SO$_4$ as the electrolyte (scan rate: 50 mV s^{-1}). The geometrically exposed electrode area was 0.196 cm^2.

the side wall of the NW surface resulting from mass transfer limitations.[17,28] In contrast to the Pt$_L$/SiNW, we used Ag particles as precursors for impregnating Pt using a galvanic exchange reaction between Ag and Pt^{2+} for 2 min, following the method reported previously,[29] resulting in the formation of Ag−Pt catalysts only at the SiNW base, denoted SiNW/Ag−Pt.

The scanning electron microscopy (SEM) images of Pt$_L$/SiNW and SiNW/Ag−Pt are shown in Figure 2. The plane and cross-sectional views showed that the Pt particles are deposited at the tips of the SiNWs in the Pt$_L$/SiNW photocathode (Figure 2a−c), whereas the pristine SiNW surface is exposed at the NW tips of the SiNW/Ag−Pt photocathode (Figure 2d−f). The pristine SiNW surface at the tips of the SiNW/Ag−Pt was simply confirmed by comparing the image with that of bare SiNWs fabricated by immersing the SiNW/Ag photocathode in concentrated HNO$_3$ to remove any metallic particles (Figure S1). Conversely, at the base of the SiNWs, the catalysts appearing as white spherical particles were only observed in the SiNW/Ag−Pt photocathode (inset in Figure 2e). The prominent metallic features in SiNW/Ag−Pt electrodes were only observed at the SiNW base, implying the dominant Pt deposition in the Ag nanoparticle (NP).

The Pt content in the Ag−Pt catalysts at the base was varied by controlling the duration of the galvanic exchange reaction of Pt^{2+} with Ag. The Pt amounts in SiNW/Ag−Pt for reaction times of 1, 2, 5, and 15 min were 0.0174, 2.04, 29.0, and 46.2 μg cm^{-2}, respectively, calculated using ICP-MS. To optimize the content of Pt in SiNW/Ag−Pt, cyclic voltammograms (CVs) were acquired in H$_2$-purged 0.5 M aqueous H$_2$SO$_4$ under simulated AM 1.5G illumination to assess the photoelectrochemical performance (Figure 3a). The SiNW/Ag−Pt photocathode obtained by 2 min of exchange reaction shows the best performance in the HER, especially in terms of the J$_{SC}$. To elucidate the origin of this trend, the total reflection spectra were acquired to measure the light absorption properties. The

absorption spectra of SiNW/Ag−Pt with 1 and 2 min of Pt impregnation are almost comparable to those of the bare SiNW (Figure 3b). In particular, the absorption spectra from the bare SiNW and SiNW/Ag−Pt with 1 min are hardly distinguishable. This implies that the lower photoelectrochemical HER performance with 1 min of galvanic exchange reaction is due to the insufficient Pt amounts for efficient HER. However, Pt impregnation times longer than 2 min result in a reduced J$_{SC}$, while the absorption increased. Based on our previous study, light is more severely absorbed in Pt than in Ag throughout the visible spectrum, resulting in energy loss as heat waste instead of being utilized to generate excitons in Si.[25] Consequently, parasitic light absorption loss by Pt is one of the origins of dwindled J$_{SC}$ at a higher Pt content in Ag−Pt catalysts. Further analysis for the verification of positive and negative effects of light absorption by the SiNW and catalysts, respectively, is underway in our laboratory using incident-photon-to-current efficiency measurements in combination with computer modeling studies.

Following the optimization of the Pt content in the catalytic Ag−Pt particles, the effect of the exposed bare Si surface area on the HER performance was investigated by varying the SiNW length via changing the Si etching time. As shown in Figures 3c and S2, the NW length increased linearly with increasing etching time, with a slope of ∼342 nm min^{-1}. The CVs for the photoelectrochemical HER in H$_2$-purged 0.5 M H$_2$SO$_4$ with different NW lengths are presented in Figure 3d. As expected, J$_{SC}$ increased with the SiNW length in the photocathodes, owing to the increased surface area for light absorption. Although the SiNW/Ag−Pt photocathode etched for 60 min still shows a slightly higher J$_{SC}$, its V$_{OC}$ slightly shifts toward the negative potential compared with that of the SiNW/Ag−Pt photocathode etched for 30 min (Table S1). We postulate that this is caused by the higher probability of charge carrier recombination in longer SiNWs. Since the bare Si surface shows low intrinsic kinetics for the HER, most of the
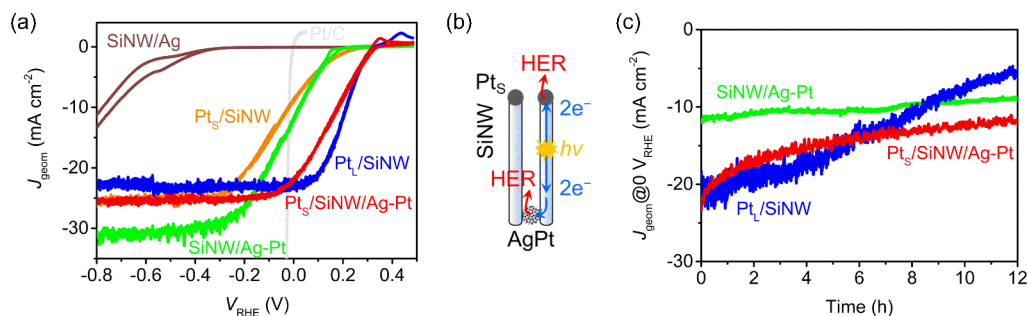
Figure 4. (a) CVs for the photoelectrochemical HER with the photocathodes, SiNW/Ag (brown line), SiNW/Ag−Pt (green line), Pt_S/SiNW (orange line), Pt_L/SiNW (blue line), and Pt_S/SiNW/Ag−Pt (red line), under simulated AM 1.5G irradiation (scan rate: 50 mV s^{-1}). CV of 20 wt % Pt/C (gray line) is also shown for comparison. (b) Schematic illustration of photogenerated electron transport to Pt_S and Ag−Pt particles located at top and base of the SiNWs, respectively. (c) Chronoamperometric curves under 0 V (vs RHE) for 12 h. The SiNW was formed by etching for the 30 min and 2 min galvanic exchange reaction (exposed electrode area: 0.196 cm^2).

photoinduced electrons can only be transferred to protons through the catalysts (see the illustration in Figure 3d).[17] Since light absorption will be more dominant at the upper part of the SiNWs and the Ag−Pt catalyst is located at the base of the SiNWs, the distance that the photogenerated electrons near the NW tip must travel to be utilized for photocurrent generation increases in longer SiNWs. In addition, the decrease in the rate of increase in J_{SC} may indirectly corroborate the inefficient charge transport by longer NWs owing to the loss of photogenerated minority carriers to charge recombination (Figure S3). Therefore, a SiNW length of ∼10 μm produced by etching for 30 min was found to be optimal for HER performance in SiNW/Ag−Pt photocathodes.

As shown in Figure 4a, the optimized SiNW/Ag−Pt electrode obtained by the 2 and 30 min galvanic exchange reaction and NW etching, respectively, exhibits a negative V_{OC} in the photoelectrochemical HER compared with the Pt_L/ SiNW photocathode fabricated by the conventional method for Pt-based SiNW photocathodes.[16,17] As discussed earlier, the Pt deposition method using conventional methods results in the dominant deposition of Pt at the NW tips, which leads to a smaller J_{SC} than that of the SiNW/Ag−Pt photocathode, owing to the parasitic light absorption or scattering by the catalysts. The lower V_{OC} of the SiNW/Ag−Pt photocathode is possibly due to the inefficient transport pathway of the photogenerated electrons for the HER, as well as the diffusion limitation through the nanochannels formed between SiNWs. To compensate for the long transport pathway, we deposited additional Pt at the tips of the SiNWs employing the same electroless deposition method used to fabricate Pt_L/SiNW. However, we lowered the amount of Pt deposited on the SiNW tips by decreasing the Pt deposition time to reduce light absorption by the catalyst particles (Pt_S/SiNW/Ag−Pt). Although J_{SC} of Pt_S/SiNW/Ag−Pt decreased slightly compared with that of SiNW/Ag−Pt, V_{OC} was indeed similar to that of Pt_L/SiNW (Figure 4a). The Pt content in Pt_S/SiNW/Ag−Pt calculated by ICP-MS analysis was 3.37 μg cm^{-2}, which is only ∼1/3 of that of Pt_L/SiNW (10.6 μg cm^{-2}). Therefore, a nearly identical photocurrent density at 0 V (vs RHE) is achieved with the Pt_S/SiNW/Ag−Pt photocathode at a lower Pt content than that in Pt_L/SiNW by optimizing the charge transport pathway along the SiNWs. In spite of the small Pt content in Ag−Pt particles, Pt is essential for consuming the photo-generated electrons by transferring them to the protons for the HER; thus, the performance of SiNW/Ag was much lower than that of SiNW/Ag−Pt (Figure 4a). In addition, the

necessity of the Ag−Pt catalyst at the base of SiNWs is also confirmed by the comparison of the voltammogram of Pt_S/ SiNW (orange line) and Pt_S/SiNW/Ag−Pt (red line). These facts indicate that Ag−Pt at the base of SiNW effectively overcomes the disadvantage of the Pt at NW tips for HER (Figure 4b), resulting in a comparable photocurrent density at 0 V (vs RHE) in Pt_S/SiNW/Ag−Pt with only ∼1/3 of Pt loading in Pt_L/SiNW.

Chronoamperometry at 0 V (vs RHE) was performed to evaluate the durability of SiNW-based photocathodes under simulated AM 1.5G illumination (Figure 4c). The geometric photocurrent density at 0 V (vs RHE) decreased continuously in the Pt_L/SiNW photocathode, as reported previously, while that in SiNW/Ag−Pt shows much better stability.[17] The catalysts on the nanostructured semiconductors easily delaminate during vigorous photocurrent density generation because nanostructuring facilitates the physical damage induced by strain in catalytic layers that occur during bubble detachment.[30] The photocurrent density at 0 V (vs RHE) in Pt_S/SiNW/Ag−Pt continuously decreased but at a lower rate than that in Pt_L/SiNW, probably owing to the geometry of catalytic sites, which were surrounded by SiNWs at the base and slightly reduced the internal strain by the smaller size of pure Pt particles at the tips.[26] In this regard, the photocurrent density at 0 V (vs RHE) in the Pt_S/SiNW/Ag−Pt photo-cathode increases above that of Pt_L/SiNW after 6 h of operation.

3. CONCLUSIONS

We demonstrated the spatial control of catalysts on hierarchical SiNW-array photocathodes for the HER by employing only a simple chemical approach involving the MACE protocol with slight modifications. Pt impregnated by galvanic replacement constituted only ∼2 μg cm^{-2} of the Ag−Pt catalyst at the base. The photoelectrochemical performance of the SiNW-based photocathodes was improved even at a lower Pt loading than that of the benchmark Pt_L/SiNW photoelectrodes by optimizing the Pt amount in the Ag−Pt catalyst particles and the SiNW length (∼10 μm), as well as by the additional small pure Pt catalysts positioned at the tips. Although the Ag−Pt catalysts at the base of the NWs are effective for preventing the absorption losses of visible light, higher Pt amounts than the optimized one in Ag−Pt catalysts result in parasitic light absorption, potentially because of the stronger optical absorptive loss at Pt than that at Ag. Optimization of the SiNW length and the additional

introduction of small amounts of pure Pt at the NW tips (Pt$_S$/ SiNW/Ag−Pt) were also conducted to reach a balance between the Si surface area and the traveling distance for charge carrier transport. By this further optimization of Pt$_S$/ SiNW/Ag−Pt, a nearly identical V_{OC} and slightly higher J_{SC} than those of the previously reported Pt$_L$/SiNW were achieved at only one-third of the Pt loading. In addition, the durability of Pt$_S$/SiNW/Ag−Pt under an applied potential of 0 V (vs RHE) was also improved when compared to that of Pt$_L$/SiNW owing to the smaller amounts of the catalyst deposited on high-curvature surfaces at the SiNW tips by relieving deleterious physical delamination during the vigorous H$_2$ formation. Although further improvement of the HER performance is desirable, especially in terms of the stability and fill factor, the results of this study can inspire the design of better catalyst/semiconductor interfaces in hierarchical 3D-structured photoelectrodes using simple chemical methods.

4. EXPERIMENTAL SECTION

4.1. SiNW Preparation. SiNWs were fabricated according to a previously reported method. Wafers of p-Si (100) (4 in., boron-doped; resistivity, 1−10 Ω cm, prime grade, single-side polished, 525 μm thickness) were purchased from Silicon Technology Corporation and first cleaned by immersion in a piranha solution (1:3 H$_2$O$_2$/H$_2$SO$_4$) for 10 min followed by washing thoroughly with deionized (DI) water (18.2 MΩ cm at 25 °C). After that, the wafers were immersed in 1% HF for 1 min to remove the surface SiO$_x$ layer, dried with N$_2$, and then transferred to a metal sputter chamber to deposit a 300 nm thick Al layer on the backside. Subsequently, the Al-deposited wafers were annealed for 30 s at 400 °C under a N$_2$ atmosphere. Before the sequential processes for SiNW fabrication, the backside of the wafers was protected by assembly in a Teflon cell. The front side of the wafer was cleaned again with the piranha solution for 1 min and washed with DI water for 3 min. Furthermore, the SiO$_x$ layer on the Si surface was removed by immersion in 5% HF for 10 s, and the front side of the wafer was directly exposed to an Ag deposition solution consisting of 10 mM AgNO$_3$ and 4.5 M HF for 1 min and finally rinsed with DI water. To form the SiNWs by the chemical etching of Si, which is facilitated by the deposited Ag seeds, the substrate was immersed in an etching solution containing 0.3 M H$_2$O$_2$ and 4.5 M HF. To optimize the NW length, the immersion time in the etching solution was controlled with designated times of 10, 20, 30, and 60 min. After etching, the substrate was rinsed thoroughly with DI water and dried under a N$_2$ stream.

4.2. Impregnation of Pt into Ag for Preparation of SiNW/Ag−Pt. The SiNW substrate with Ag particles at the base was immersed in 30 mL of an aqueous polyvinylpyrrolidone (PVP, 0.27 g mL^{-1}, average $M_w \sim 40\,000$) solution for 30 min at 80 °C. Then, 30 mL of a Pt deposition solution containing 10 mM K$_2$PtCl$_4$ and 100 mM HCl was added to the PVP solution for the galvanic exchange of Ag with Pt^{2+}. After the designated reaction time, the SiNW/Ag−Pt electrode was rinsed thoroughly with ethanol and DI water.

4.3. Electroless Pt Deposition at the NW Tips to Form Pt$_L$/SiNW and Pt$_S$/SiNW/Ag−Pt. The SiO$_x$ on the SiNW-based photocathodes was removed by immersion in a 5% HF solution for 20 s, followed by immersion in an aqueous solution consisting of 1 mM H$_2$PtCl$_6$ and 0.4 M HF for 20 s to deposit Pt at the SiNW tips. Afterward, the photoelectrodes were washed with DI water. For the formation of Pt$_L$ at the

tips, this deposition procedure was consecutively performed three times, while it was conducted only once for acquiring Pt$_S$ to prepare Pt$_S$/SiNW/Ag−Pt.

■ ASSOCIATED CONTENT

ⓈI Supporting Information

The Supporting Information is available free of charge at https://pubs.acs.org/doi/10.1021/acsomega.1c03014.

Experimental methods, SEM image of bare SiNW, cross-sectional SEM images of SiNW/Ag−Pt, effect of the length of the SiNWs on saturated photocurrent density, relation between J_{SC} and the NW length, and table for parameters of photoelectrochemical performance (PDF)

■ AUTHOR INFORMATION

Corresponding Authors

Sung Yul Lim − *Department of Chemistry and Research Institute for Basic Science, Kyung Hee University, Seoul 02447, Korea;* ⓞ orcid.org/0000-0002-2838-6967; Email: limsy@khu.ac.kr

Taek Dong Chung − *Department of Chemistry, Seoul National University, Seoul 08826, Korea;* ⓞ orcid.org/ 0000-0003-1092-8550; Email: tdchung@snu.ac.kr

Authors

Daye Seo − *Department of Chemistry, Seoul National University, Seoul 08826, Korea*

Min Seok Jang − *School of Electrical Engineering, Korea Advanced Institute Science and Technology (KAIST), Daejeon 34141, Korea;* ⓞ orcid.org/0000-0002-5683-1925

Complete contact information is available at: https://pubs.acs.org/10.1021/acsomega.1c03014

Notes

The authors declare no competing financial interest.

■ REFERENCES

(1) Kemppainen, E.; Bodin, A.; Sebok, B.; Pedersen, T.; Seger, B.; Mei, B.; Bae, D.; Vesborg, P. C. K.; Halme, J.; Hansen, O.; Lund, P. D.; Chorkendorff, I. Scalability and feasibility of photoelectrochemical H$_2$ evolution: The ultimate limit of Pt nanoparticle as an HER catalyst. *Energy Environ. Sci.* **2015**, *8*, 2991−2999.

(2) Kempler, P. A.; Coridan, R. H.; Lewis, N. S. Effects of bubbles on the electrochemical behavior of hydrogen-evolving Si microwire arrays oriented against gravity. *Energy Environ. Sci.* **2020**, *13*, 1808−1817.

(3) Fu, H. C.; Varadhan, P.; Lin, C. H.; He, J. H. Spontaneous solar water splitting with decoupling of light absorption and electrocatalysis using silicon back-buried junction. *Nat. Commun.* **2020**, *11*, No. 3930.

(4) Quinn, J.; Hemmerling, J.; Linic, S. Guidelines for Optimizing the Performance of Metal-Insulator-Semiconductor (MIS) Photoelectrocatalytic Systems by Tuning the Insulator Thickness. *ACS Energy Lett.* **2019**, *4*, 2632−2638.

(5) Ardo, S.; Rivas, D. F.; Modestino, M. A.; Greiving, V. S.; Abdi, F. F.; Alarcon Llado, E.; Artero, V.; Ayers, K.; Battaglia, C.; Becker, J.-P.; Bederak, D.; Berger, A.; Buda, F.; Chinello, E.; Dam, B.; Di Palma, V.; Edvinsson, T.; Fujii, K.; Gardeniers, H.; Geerlings, H.; Hashemi, S. M. H.; Haussener, S.; Houle, F.; Huskens, J.; James, B. D.; Konrad, K.; Kudo, A.; Kunturu, P. P.; Lohse, D.; Mei, B.; Miller, E. L.; Moore, G. F.; Muller, J.; Orchard, K. L.; Rosser, T. E.; Saadi, F. H.; Schuttauf, J.-W.; Seger, B.; Sheehan, S. W.; Smith, W. A.; Spurgeon, J.; Tang, M. H.; Van De Krol, R.; Vesborg, P. C. K.; Westerik, P. Pathways to electrochemical solar-hydrogen technologies. *Energy Environ. Sci.* **2018**, *11*, 2768−2783.

(6) Tseng, Y. M.; Gu, R. Y.; Cheng, S. L. Design and fabrication of vertically aligned single-crystalline Si nanotube arrays and their enhanced broadband absorption properties. *Appl. Surf. Sci.* **2020**, *508*, No. 145223.

(7) Qiao, L.; Liao, M. J.; Wu, J. X.; Jiang, Q. M.; Zhang, Y. H.; Li, Y. H. Molybdenum disulfide/silver/p-silicon nanowire heterostructure with enhanced photoelectrocatalytic activity for hydrogen evolution. *Int. J. Hydrogen Energy* **2018**, *43*, 22235−22242.

(8) Moreno-Hernandez, I. A.; Yalamanchili, S.; Fu, H. J.; Atwater, H. A.; Brunschwig, B. S.; Lewis, N. S. Conformal SnO_x heterojunction coatings for stabilized photoelectrochemical water oxidation using arrays of silicon microcones. *J. Mater. Chem. A* **2020**, *8*, 9292−9301.

(9) Vijselaar, W.; Tiggelaar, R. M.; Gardeniers, H.; Huskens, J. Efficient and Stable Silicon Microwire Photocathodes with a Nickel Silicide Interlayer for Operation in Strongly Alkaline Solutions. *ACS Energy Lett.* **2018**, *3*, 1086−1092.

(10) Li, L. J.; Wu, S. L.; Zhou, Z. Y.; Guo, P. J.; Li, X. F. Size-dependent performances in homogeneous, controllable, and large-area silicon wire array photocathode. *J. Power Sources* **2020**, *473*, No. 228580.

(11) Lim, S. Y.; Kim, Y. R.; Ha, K.; Lee, J. K.; Lee, J. G.; Jang, W.; Lee, J. Y.; Bae, J. H.; Chung, T. D. Light-guided electrodeposition of non-noble catalyst patterns for photoelectrochemical hydrogen evolution. *Energy Environ. Sci.* **2015**, *8*, 3654−3662.

(12) Chen, Y. K.; Sun, K.; Audesirk, H.; Xiang, C. X.; Lewis, N. S. A quantitative analysis of the efficiency of solar-driven water-splitting device designs based on tandem photoabsorbers patterned with islands of metallic electrocatalysts. *Energy Environ. Sci.* **2015**, *8*, 1736−1747.

(13) Shaner, M. R.; McKone, J. R.; Gray, H. B.; Lewis, N. S. Functional integration of Ni-Mo electrocatalysts with Si microwire array photocathodes to simultaneously achieve high fill factors and light-limited photocurrent densities for solar-driven hydrogen evolution. *Energy Environ. Sci.* **2015**, *8*, 2977−2984.

(14) Kempler, P. A.; Gonzalez, M. A.; Papadantonakis, K. M.; Lewis, N. S. Hydrogen Evolution with Minimal Parasitic Light Absorption by Dense Co-P Catalyst Films on Structured p-Si Photocathodes. *ACS Energy Lett.* **2018**, *3*, 612−617.

(15) Boettcher, S. W.; Warren, E. L.; Putnam, M. C.; Santori, E. A.; Turner-Evans, D.; Kelzenberg, M. D.; Walter, M. G.; McKone, J. R.; Brunschwig, B. S.; Atwater, H. A.; Lewis, N. S. Photoelectrochemical Hydrogen Evolution Using Si Microwire Arrays. *J. Am. Chem. Soc.* **2011**, *133*, 1216−1219.

(16) Oh, I.; Kye, J.; Hwang, S. Enhanced Photoelectrochemical Hydrogen Production from Silicon Nanowire Array Photocathode. *Nano Lett.* **2012**, *12*, 298−302.

(17) Dai, P. C.; Xie, J.; Mayer, M. T.; Yang, X. G.; Zhan, J. H.; Wang, D. W. Solar Hydrogen Generation by Silicon Nanowires Modified with Platinum Nanoparticle Catalysts by Atomic Layer Deposition. *Angew. Chem., Int. Ed.* **2013**, *52*, 11119−11123.

(18) Dasgupta, N. P.; Liu, C.; Andrews, S.; Prinz, F. B.; Yang, P. D. Atomic Layer Deposition of Platinum Catalysts on Nanowire Surfaces for Photoelectrochemical Water Reduction. *J. Am. Chem. Soc.* **2013**, *135*, 12932−12935.

(19) Bellani, S.; Antognazza, M. R.; Bonaccorso, F. Carbon-Based Photocathode Materials for Solar Hydrogen Production. *Adv. Mater.* **2019**, *31*, No. 1801446.

(20) Vijselaar, W.; Westerik, P.; Veerbeek, J.; Tiggelaar, R. M.; Berenschot, E.; Tas, N. R.; Gardeniers, H.; Huskens, J. Spatial decoupling of light absorption and catalytic activity of Ni-Mo-loaded high-aspect-ratio silicon microwire photocathodes. *Nat. Energy* **2018**, *3*, 185−192.

(21) Osberg, K. D.; Schmucker, A. L.; Senesi, A. J.; Mirkin, C. A. One-Dimensional Nanorod Arrays: Independent Control of Composition, Length, and Interparticle Spacing with Nanometer Precision. *Nano Lett.* **2011**, *11*, 820−824.

(22) Ozel, T.; Ashley, M. J.; Bourret, G. R.; Ross, M. B.; Schatz, G. C.; Mirkin, C. A. Solution-Dispersible Metal Nanorings with Deliberately Controllable Compositions and Architectural Parameters for Tunable Plasmonic Response. *Nano Lett.* **2015**, *15*, 5273−5278.

(23) Wendisch, F. J.; Abazari, M.; Werner, V.; Barb, H.; Rey, M.; Goerlitzer, E. S. A.; Vogel, N.; Mahdavi, H.; Bourret, G. R. Spatioselective Deposition of Passivating and Electrocatalytic Layers on Silicon Nanowire Arrays. *ACS Appl. Mater. Interfaces* **2020**, *12*, 52581−52587.

(24) Chong, L.; Wen, J. G.; Kubal, J.; Sen, F. G.; Zou, J. X.; Greeley, J.; Chan, M.; Barkholtz, H.; Ding, W. J.; Liu, D. J. Ultralow-loading platinum-cobalt fuel cell catalysts derived from imidazolate frameworks. *Science* **2018**, *362*, 1276−1281.

(25) Lim, S. Y.; Ha, K.; Ha, H.; Lee, S. Y.; Jang, M. S.; Choi, M.; Chung, T. D. Three-dimensionally patterned Ag-Pt alloy catalyst on planar Si photocathodes for photoelectrochemical H_2 evolution. *Phys. Chem. Chem. Phys.* **2019**, *21*, 4184−4192.

(26) Kim, J.; Park, H.; Hannon, J. B.; Bedell, S. W.; Fogel, K.; Sadana, D. K.; Dimitrakopoulos, C. Layer-Resolved Graphene Transfer via Engineered Strain Layers. *Science* **2013**, *342*, 833−836.

(27) Li, M. C.; Li, Y. F.; Liu, W. J.; Yue, L.; Li, R. K.; Luo, Y. N.; Trevor, M.; Jiang, B.; Bai, F.; Fu, P. F.; Zhao, Y.; Shen, C.; Mbengue, J. M. Metal-assisted chemical etching for designable monocrystalline silicon nanostructure. *Mater. Res. Bull.* **2016**, *76*, 436−449.

(28) Bao, X. Q.; Cerqueira, M. F.; Alpuim, P.; Liu, L. F. Silicon nanowire arrays coupled with cobalt phosphide spheres as low-cost photocathodes for efficient solar hydrogen evolution. *Chem. Commun.* **2015**, *51*, 10742−10745.

(29) Zhang, W. Q.; Yang, J. Z.; Lu, X. M. Tailoring Galvanic Replacement Reaction for the Preparation of Pt/Ag Bimetallic Hollow Nanostructures with Controlled Number of Voids. *ACS Nano* **2012**, *6*, 7397−7405.

(30) Kou, T. Y.; Wang, S. W.; Li, Y. Perspective on High-Rate Alkaline Water Splitting. *ACS Mater. Lett.* **2021**, *3*, 224−234.